Liang Zhu
Department of Mechanical Engineering,
University of Maryland, Baltimore County,
1000 Hilltop Circle,
Baltimore, MD 21227
e-mail: zliang@umbc.edu

Lisa X. Xu
School of Mechanical Engineering,
Purdue University,
West Lafayette, IN 47907

Qinghong He
Department of Mechanical Engineering,
University of Maryland Baltimore County,
Baltimore, MD 21227

Sheldon Weinbaum
Department of Mechanical Engineering,
City College of The City University of New York,
New York, NY 10031

A New Fundamental Bioheat Equation for Muscle Tissue—Part II: Temperature of SAV Vessels

In this study, a new theoretical framework was developed to investigate temperature variations along countercurrent SAV blood vessels from 300 to 1000 μm diameter in skeletal muscle. Vessels of this size lie outside the range of validity of the Weinbaum-Jiji bioheat equation and, heretofore, have been treated using discrete numerical methods. A new tissue cylinder surrounding these vessel pairs is defined based on vascular anatomy, Murray's law, and the assumption of uniform perfusion. The thermal interaction between the blood vessel pair and surrounding tissue is investigated for two vascular branching patterns, pure branching and pure perfusion. It is shown that temperature variations along these large vessel pairs strongly depend on the branching pattern and the local blood perfusion rate. The arterial supply temperature in different vessel generations was evaluated to estimate the arterial inlet temperature in the modified perfusion source term for the s vessels in Part I of this study. In addition, results from the current research enable one to explore the relative contribution of the SAV vessels and the s vessels to the overall thermal equilibration between blood and tissue. [DOI: 10.1115/1.1431263]

1 Introduction

Several bioheat transfer models are currently used to examine the effect of microvascular blood flow and/or vascular geometry on the local heat transfer [1–3]. These continuum models collectively describe the temperature distribution over a representative control volume, whose size is much larger than the scale of the thermally significant blood vessels and much smaller than the scale of the whole tissue. Due to the large range in size of the thermally significant vessels, it is difficult to define such a control volume. The regions of validity of these continuum models have been extensively discussed and clarified in the past [4–12]. Further, in applications where point to point temperature nonuniformities are required near discrete large vessels, vascular models are necessary to accurately predict the tissue temperature field. As expected, Crezee and Lagendijk [13] have found that blood flow in large, thermally unequilibrated vessels is the main cause of temperature inhomogeneity during hyperthermia treatment.

In this paper, we will examine the thermal equilibration of blood in vessels between 300 μm and 1000 μm in diameter to determine their contribution to the total blood-tissue heat exchange. Lemons et al. [9] have shown that vessels in this size range occur nearly exclusively as countercurrent pairs in skeletal muscle and have a thermal signature indicating that they undergo partial thermal equilibration with the surrounding tissue. These countercurrent vessels are often referred to as supply artery-vein pairs or SAV vessels in muscle tissue. They lie outside the range of validity of the Weinbaum-Jiji equation, which experiments and theory [14,15] have demonstrated, is limited to countercurrent vessel pairs of $<$200 μm diameter. At present, there is no adequate theory for describing the thermal contribution of these large blood vessels, and they are too numerous to be individually treated in numerical simulations. This paper is Part II of a two-part investigation in which a new basic model is developed for blood-tissue heat transfer in skeletal muscle tissue. Part I was confined to *s* vessel tissue cylinders and vessels less than 300 μm diameter.

It is well known that the Pennes perfusion source term overestimates the actual blood perfusion effect in tissue in two ways. First, it considers that all the heat leaving the artery is absorbed by the local tissue and there is no venous rewarming. It has been suggested by previous researchers [16,17] that a ''correction coefficient'' which is less than unity and accounts for venous rewarming should multiply the Pennes perfusion term. A correction coefficient which is close to zero implies a significant countercurrent rewarming of the paired vein and a coefficient of unity no rewarming. In Part I of this study [18], a new model for muscle tissue heat transfer was developed using Myrhage and Eriksson's description [19] of a muscle tissue cylinder surrounding countercurrent secondary vessels (*s* vessels) as the basic heat transfer unit. The thermal equilibration of the returning blood in the *s* vein was rigorously analyzed to determine the venous return temperature in the tissue cylinder. This led to a modified Pennes bioheat equation with a new perfusion source term, which can be used to predict average tissue temperature distribution in muscle tissue regions containing vessels less than 300 μm in diameter. It has been shown that for most muscle tissues, the ''correction coefficient'' varies between 0.6 to 0.8 suggesting that there is 20 percent to 40 percent venous rewarming in the *s* vessel-tissue cylinder. A second limitation of the Pennes perfusion source term is that the arterial temperature is assumed to be equal to the body core temperature. Based on the analysis in Part I this arterial temperature should be the local SAV artery temperature at the inlet of the *s* vessel tissue cylinder. SAV vessels of 1000 to 300 μm diameter achieve only partial thermal equilibration with the surrounding tissue which is then completed when the blood enters the *s* vessel tissue cylinders. It is, thus, necessary to study the thermal equilibration along these partially equilibrated larger blood vessels if we wish to determine the relative importance of the SAV vessels and the *s* vessels in the overall heat exchange.

As sketched in Fig. 1, the *s* vessel tissue cylinder is supplied by the *P* vessels which branch off from the SAV vessel pairs. The *P* vessels are relatively short and thus, the local arterial inlet temperature appearing in the modified Pennes source term is well approximated by the local arterial temperature in the SAV vessel pair. This temperature depends not only on the interaction between the countercurrent SAV vessels but also on the local tissue temperature distribution. The SAV vessels bifurcate from the major branching arteries that emanate from the central supply vessels that run along the axis of the limb. A central question in analyzing

Contributed by the Bioengineering Division for publication in the JOURNAL OF BIOMECHANICAL ENGINEERING. Manuscript received by the Bioengineering Division Oct. 17, 2000; revised manuscript received Aug. 16, 2001. Associate Editor: J. J. McGrath.

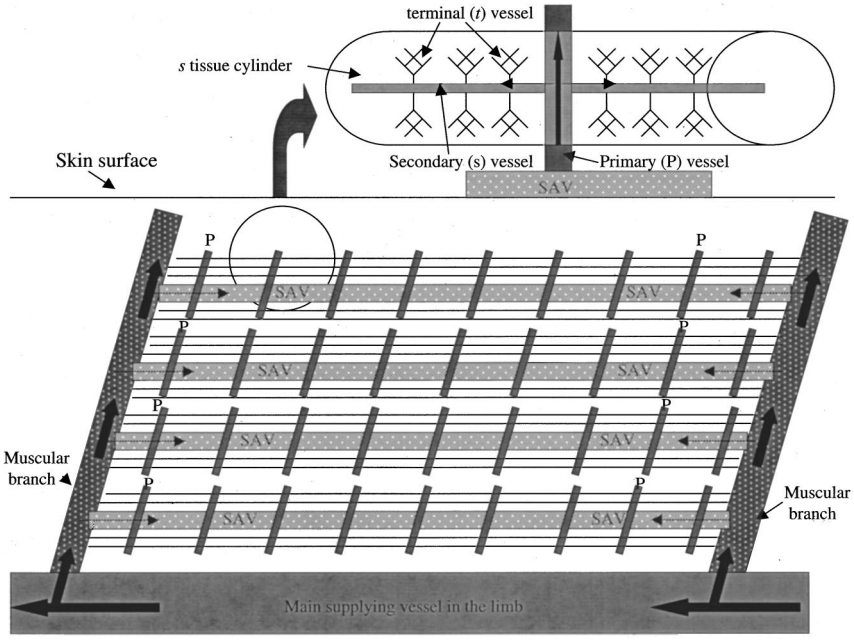

Fig. 1 Proposed vasculature showing the relationship between the muscular arteries, the SAV tissue cylinder, and the *s* tissue cylinder in a human limb

the countercurrent equilibration in the SAV vessels is to determine how much thermal energy leaving the artery returns to the countercurrent vein and how much is lost to the surrounding tissue. This redistribution of energy is a function of the local tissue temperature distribution and the vascular geometry. The anatomic structure of the microvascular bed in the *s* vessel tissue cylinder and our modified Pennes equation were presented in Part I of this study. In Part II we primarily focus on the SAV vessel pairs.

Anatomically, the *P*, *s*, and *t* vessels are the first three branches of the final generations of a branching network that was initially described in peripheral muscle tissue in Weinbaum et al. [3]. This network is part of a space filling structure for all muscle tissue. A typical circulatory system in a human limb is fed mainly by one or two major pairs of countercurrent arteries and veins that run axially along the limb. As schematically illustrated in Fig. 1, the blood vessels, which branch off from the main axial supply vessels, are defined as the muscular branches. These large branches run obliquely toward the skin surface and supply the large muscle bundles in skeletal muscle. These large bundles are supplied by the SAV vessel pairs which run along the length of the muscle. Several hundred small *s* vessel tissue cylinders comprise each large muscle bundle. The muscular branches and the SAV vessels decrease in size from approximately 1000 μm diameter and approach 300 μm diameter when they encounter the *P* vessels under normal conditions in a human limb. A single SAV vessel pair supplies numerous *P* vessels and thus a multitude of *s* vessel tissue cylinders, as previously discussed in Weinbaum et al. [18]. The *s* vessels, the *P* vessels, and the SAV vessels form a space-filling countercurrent network characteristic of all muscle tissues.

The temperature distribution in the SAV vessels is mainly determined by the thermal interaction between the SAV vessel pair and its surrounding tissue, and by the temperature distribution in the muscular branches. Like the *s* vessels, the SAV vessels are not perfect countercurrent heat exchangers. If these vessels were buried in infinitely deep tissue all the energy lost from the SAV artery would enter the SAV vein. The presence of thermal interaction between SAV pairs and the free surface can cause an asymmetry of this energy transfer. Some of the thermal energy leaving the SAV artery does not enter the SAV vein. Because of their large size, the thermal equilibration in the SAV vessels is at the most only partial and the equilibration length will increase at higher flow rates in an exercising muscle. We intend to characterize this equilibration for the first time and obtain realistic estimates for T_{ab} as a function of branching distance from the axial vessels that run along the length of the limb.

Strictly speaking, an investigation of the temperature distribution in the SAV vessels requires the knowledge of the thermal interaction between all the blood vessels and tissue, which is impractical. In this paper, contributions of the *P* vessels and their *s* vessel branches to the total heat exchange are treated as a continuous bleed-off from the SAV vessel pair (see Fig. 1). The spacing of the large SAV vessels was never fully described in previous investigations that attempted to develop a model for the deep muscle tissue of the limb. Our solution approach for determining the temperature decay in the SAV vessel pair is a two-step procedure. First, a large tissue cylinder surrounding the SAV vessel pair is defined using a new scaling analysis which combines anatomical analysis, Murray's law and the assumption of uniform perfusion. This analysis leads to a generalized anatomic description of both the SAV vessel pair and its tissue cylinder geometry. Second, the boundary value problem for the thermal interaction between the SAV vessels and the tissue cylinder is solved for the two vascular branching patterns shown in Fig. 2. These branching patterns, which we describe next, represent two limits of possible thermal interaction between blood vessels and tissue.

2 Description of the SAV Tissue Cylinder

Unlike the vascular arrangements of blood vessels less than 300 μm in diameter, which have been studied in detail for different muscle tissues, there is no systematic description in the literature of vessel branching patterns for vessels between 300 and 1000 μm in diameter. Generally speaking, the branching patterns for the muscular branches and SAV vessels in humans and mammals are either one or a combination of the two general patterns shown in Fig. 2. The axial variation of the blood vessel radius "*a*" and the SAV tissue cylinder radius R_t surrounding the vessels can be determined by introducing flow continuity and several other physiological constraints as follows.

The first pattern (Fig. 2(*a*)) is called "pure branching." In this pattern one vessel branches to form two equal vessels in each successive generation and there is no capillary bleedoff from the

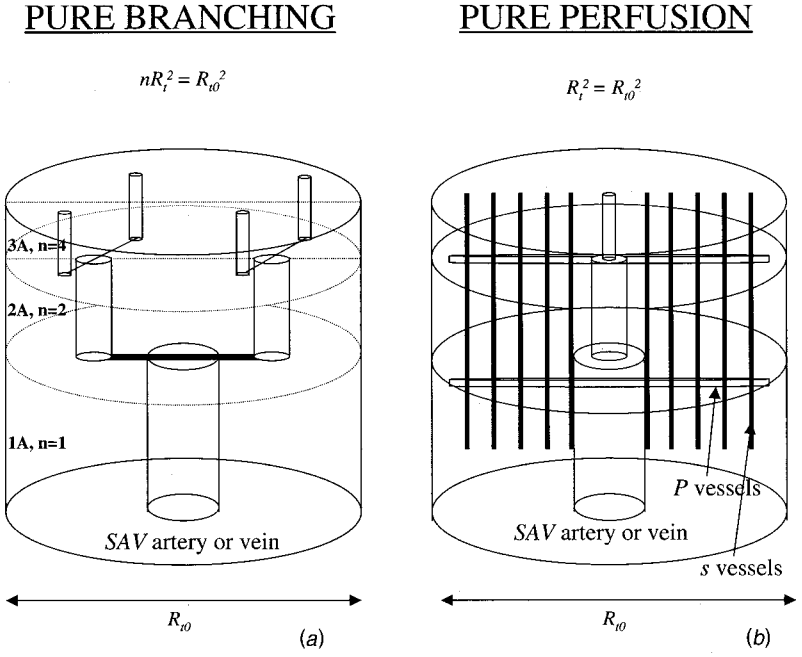

Fig. 2 Two vascular branching patterns for the SAV vessel pairs. Note that either the countercurrent SAV artery or vein is shown.

vessels. This pattern has been observed in skeletal muscle in the rat [20] and is also prevalent in the first few bifurcations from the main supply vessels in a muscle that does not have an extended axial structure. During exercise, the blood flow can be redistributed and directly transported to the cutaneous layer without perfusing the surrounding tissue. The SAV vessels in the pure branching pattern can be viewed as a tapered vessel pair consisting of the vessel branches from all previous generations which contains one branch in each vessel generation. If one assumes that the vessel bifurcates into two equal-sized branches, the ratio of the blood flow rate in the mother vessel to that in the daughter vessel should be a constant based on mass conservation; thus, $2Q_{i+1}=Q_i$. Mathematical rearrangement of this relationship leads to $Q_{i+1}-Q_i/L_i=-Q_{i+1}/L_i$, where L_i is the length of vessel generation i. If one assumes that the left side of the above relationship can be approximated as dQ/dz, the above equation can be rewritten as $dQ/dz=-Q/L_i$. Combining this relationship with Murray's law, $Q\propto a^3$, one finds that $3a^2(da/dz)=-a^3/L_i$. The vessel length L_i, in general, decreases with the vessel radius a. Previous experimental measurements of the blood vessel length L_i and the vessel radius a by Song et al. [14] led to an empirical expression, $L_i(mm)=0.067a^{1.102}(\mu m)$ for blood vessels less than 200 μm in diameter in skeletal muscle. Here we extrapolate this expression to larger blood vessels ranging from 300 to 1000 μm in diameter. Whitmore's data for a 20 kg dog [21] shows that this relationship provides a reasonable fit for all vessels up to 1 mm diameter. Therefore, substituting L_i into the above relationship, one obtains

$$\frac{da}{dz}=-\frac{a^{-0.102}}{0.02012}. \tag{1}$$

The axial variation of vessel radius "a" can then be determined by integrating Eq. (1) with an initial radius a_0 at $z=0$.

Flow continuity requires that $nQ=$constant, where $n=1,2,4,8$, etc. is the number of artery-vein pairs in each succeeding generation. When it is combined with Murray's law, $Q\propto a^3$, n will scale as $n\propto 1/a^3$. In the pure branching pattern we require that the total tissue cross-sectional area surrounding all vessels in each generation remain constant. Thus, if R_t is the local radius of the tissue cylinder surrounding a vessel pair and πR_t^2 is its cross-sectional area, this cross-sectional area is halved each time a vessel divides as shown in Fig. 2(a). A single vessel in generation 1 will have its tissue cylinder cross-sectional area first shared by two, then four vessels, and so forth, as it continues to bifurcate. Thus, nR_t^2 is a constant. Combining the requirements $nR_t^2=$constant and $n\propto 1/a^3$, one finds that $R_t^2\propto a^3$ and the axial variation of R_t can be determined from a. The integrated Eq. (1) and these scaling relations require that the vessel radius a, blood velocity u, and tissue cylinder radius R_t satisfy

$$a=\sqrt[1.102]{-5.5z+a_0^{1.102}},\quad u=u_0(a/a_0),\quad R_t=R_{t0}(a/a_0)^{3/2} \tag{2}$$

where the subscript 0 represents values at the entrance ($z=0$) of the tissue cylinder.

The second branching pattern shown in Fig. 2(b) is called "pure perfusion." In this branching pattern the SAV vessel tapers as the smaller vessels branch from the main axial vessels. This pattern describes the SAV vessel branching pattern shown in Fig. 1 for the long axial muscles in the human limb. The smaller vessels branching from the SAV vessels are the P vessels, which then supply the subsequent s vessel tissue cylinders. In this case there is only one SAV vessel pair and the corresponding tissue cylinder surrounding it is of uniform radius in the axial direction. Murray's law requires that the local blood flow rate Q is proportional to the cube of vessel radius, $Q\propto a^3$. If uniform perfusion is assumed in the local tissue cylinder surrounding the SAV vessels, then one requires that $dQ/dz\propto R_t^2$. Combining the uniform perfusion assumption and Murray's law, one obtains

$$a^2(da/dz)\propto R_t^2. \tag{3}$$

For a long muscle of constant radius, $R_t=R_{t0}$, Eq. (3) leads to $da/dz\propto a^{-2}$. In this case, the axial variations of a, u, and R_t are expressed as

$$a=a_0\sqrt[3]{1-z/C},\quad u=u_0\sqrt[3]{1-z/C},\quad R_t=R_{t0} \tag{4}$$

where C is a constant determined by the vessel length and the change in vessel radius between $z=0$ and $z=L$ which will be calculated later.

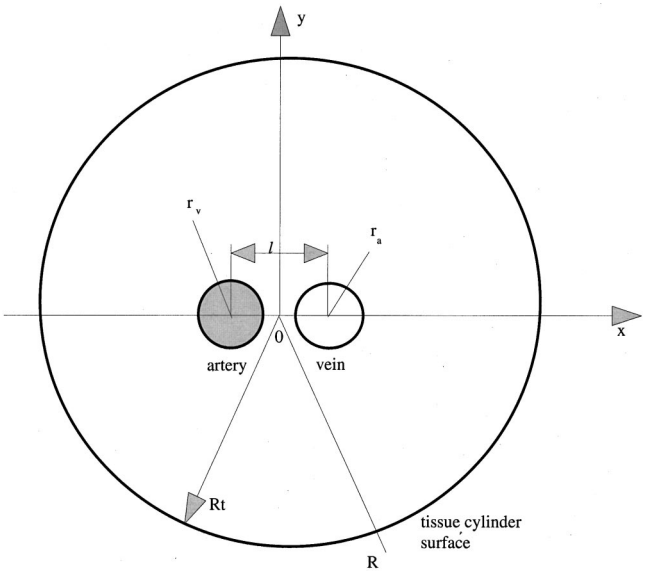

Fig. 3 The geometry of the cross-sectional plane and coordinate system in the tissue cylinder

3 Mathematic Formulation

One tapered countercurrent SAV vessel pair (SAV vessels) is considered in each tissue cylinder. The axial variation of the geometry is determined either by Eqs. (2) or (4). Referring to Fig. 3, the principal simplifying assumptions of the model are (i) both the flow and temperature fields are steady; (ii) the SAV artery and vein are located symmetrically in the cross-sectional plane. To simplify the analysis in the cross-sectional plane, the artery and vein are assumed to be of the same size, the same blood flow velocity, and the same vessel eccentricity. Thus, one has

$$\begin{gathered} a_a^*=a_v^*=a^*(z), \quad a_a^*|_{z=0}=a_v^*|_{z=0}=a_0^* \\ u_a^*=u_v^*=u^*(z), \quad u_a^*|_{z=0}=u_v^*|_{z=0}=u_0^* \\ s_a^*=s_v^*=s^*(z), \quad l_{a-v}^*(z)=2s^*. \end{gathered} \tag{5}$$

Here the subscripts a, v refer to the SAV artery and vein, respectively. Asterisks denote dimensional variables or parameters. s^* is the vessel eccentricity, and l^* is the vessel center to center spacing; (iii) the effect of branching from the SAV vessel in Fig. 2(b) is treated as a continuous bleedoff from the SAV pairs; (iv) We assume that the vessel eccentricity and the vessel center to center spacing follow the same axial variation as the vessel radius. The requirement of uniform perfusion provides a relationship between a_0^*, L^*, and R_{t0}^*. These assumptions, when combined with Eq. (2) and Eq. (4), lead to the following expressions:

pure branching pattern

$$\begin{gathered} a^*(z^*)=\sqrt[1.102]{-5.5z^*+a_0^{*1.102}}, \quad u^*=u_0^*(a^*/a_0^*), \\ R_t^*=R_{t0}^*(a^*/a_0^*)^{3/2} \\ s^*(z^*)=s_0^*(a^*/a_0^*), \quad l^*(z^*)=l_0^*(a^*/a_0^*) \end{gathered} \tag{6}$$

and

pure perfusion pattern

$$\begin{gathered} a^*=a_0^*\sqrt[3]{1-z^*/C^*}, \quad u^*=u_0^*\sqrt[3]{1-z^*/C^*}, \quad R_t^*=R_{t0}^* \\ C^*=L^*/[1-(a_e^*/a_0^*)^3], \quad s^*(z^*)=s_0^*a^*/a_0^*, \\ l^*(z^*)=l_0^*a^*/a_0^* \end{gathered} \tag{7}$$

where L^* is the cylinder length, a_0^* is the vessel radius at $z^*=0$ and a_e^* is the vessel radius at $z^*=L^*$; (v) the velocity field in the blood vessels can be obtained by solving the Navier-Stokes equations for an incompressible fluid. Similar to the analysis given in Part I, one obtains parabolic expressions for the velocity profile in the axial direction of the vessels; (vi) axial conduction is neglected in the vessel region due to the high blood flow rates [22]. However, axial conduction in the tissue region is considered. $\partial^2 T_t^*/\partial z^{*2}$ is approximated by its value on the tissue cylinder surface, $d^2T_{t\text{local}}^*/dz^{*2}$; (vii) the temperature gradient $\partial T_{a,v}/\partial z$ in the convective terms of the vessel energy equations can be approximated by the axial gradient of the vessel bulk temperatures, $dT_{ab,vb}/dz$, as previously justified [22].

The nondimensional parameters and variables are defined as

$$\begin{gathered} s_{a,v}=\frac{s_{a,v}^*}{a_0^*}, \quad r_{a,v}=\frac{r_{a,v}^*}{a_0^*}, \quad a_{a,v}=\frac{a_{a,v}^*}{a_0^*}, \quad l=\frac{l^*}{a_0^*}, \quad R=\frac{R^*}{a_0^*}, \\ R_t=\frac{R_t^*}{a_0^*}, \quad C=\frac{C^*}{a_0^*}, \quad z=\frac{z^*}{a_0^*}, \quad L=\frac{L^*}{a_0^*}, \\ u_{a,v}=\frac{u_{a,v}^*}{u_0^*}, \quad \mathrm{Pe}_0=\frac{2\rho_f C_f a_0^* u_0^*}{k_f}, \quad T_{a,v,t}=\frac{T_{a,v,t}^*-T_{t\text{local}}^*(z)}{T_{ab0}^*-T_{t\text{local}}^*(L)}, \\ F(z)=\frac{T_{t\text{local}}^*(z)}{T_{ab0}^*-T_{t\text{local}}^*(z)}. \end{gathered} \tag{8}$$

The dimensionless tissue temperature T_t is defined such that $T_t=0$ at the cylinder surface. All length variables are scaled by the vessel radius a_0^* at $z^*=0$. T_{ab0}^* is the artery bulk temperature at $z^*=0$. The tissue temperature on the outer tissue cylinder boundary $T_{t\text{local}}^*$ is prescribed and need not be constant. The function $F(z)$ is determined by the prescribed $T_{t\text{local}}^*$. Employing these assumptions, one can rewrite the dimensionless energy equations for the blood vessels and the tissue as given in Weinbaum et al. [18]

$$\begin{gathered} \frac{1}{r_{a,v}}\frac{\partial}{\partial r_{a,v}}\left(r_{a,v}\frac{\partial T_{a,v}}{\partial r_{a,v}}\right)+\frac{1}{r_{a,v}^2}\frac{\partial^2 T_{a,v}}{\partial \phi_{a,v}^2} \\ =f\,\mathrm{Pe}_0 u_{a,v}\left(1-\frac{r_{a,v}^2}{a_{a,v}^2}\right)\left(\frac{dT_{ab,vb}}{dz}+\frac{dF}{dz}\right), \\ r_{a,v}\leqslant a_{a,v}(z), \quad z\leqslant L \\ f=1 \quad \text{for artery;} \quad f=-1 \quad \text{for vein} \end{gathered} \tag{9}$$

$$\begin{gathered} \frac{1}{R}\frac{\partial}{\partial R}\left(R\frac{\partial T_t}{\partial R}\right)+\frac{1}{R^2}\frac{\partial^2 T_t}{\partial \phi^2}=-\frac{d^2F(z)}{dz^2}+BP[T_{ab}(z)-F(z)], \\ R\leqslant R_t(z), \quad r_{a,v}\geqslant a_{a,v}(z) \\ BP=0 \quad \text{for pure branching pattern;} \\ BP=\frac{0.7\omega\rho_f C_f a_{a0}^{*2}}{k_t} \quad \text{for pure perfusion pattern} \end{gathered} \tag{10}$$

where ω is the local blood perfusion rate due to the bleedoff in the pure perfusion pattern. The Pennes-like source term [18] on the right side of Eq. (10) for the pure perfusion pattern takes into consideration the net heat release due to countercurrent heat exchange in the s vessel tissue cylinder, as described in Part I. The overall heat released by the bleedoff should be proportional to the temperature difference between the SAV artery and tissue, multiplied by a ''correction coefficient'' to account for the venous rewarming in the s vessel tissue cylinder. 0.7 is an average value of the correction coefficient calculated by Weinbaum et al. [18] for various muscle tissues.

The continuity of temperature and heat flux on the vessel surfaces and the convection boundary condition on the tissue cylinder surface require that

$$\begin{cases} T_{a,v}=T_t, & \text{for } r_{a,v}=a_{a,v}(z) \\ \dfrac{\partial T_{a,v}}{\partial r_{a,v}}=\dfrac{\partial T_t}{\partial r_{a,v}}, & \text{for } r_{a,v}=a_{a,v}(z) \end{cases} \tag{11}$$

$$T_t=0, \quad \text{for } R=R_t \tag{12}$$

In Eq. (9), T_{ab} and T_{vb} are the artery and vein bulk temperatures, respectively. These bulk temperatures are defined as

$$T_{ab,vb}=\frac{2}{\pi a_{a,v}}\int_{-\pi}^{\pi}\int_{0}^{a_{a,v}} T_{a,v}\left(1-\frac{r_{a,v}^2}{a_{a,v}^2}\right) r_{a,v}\,dr_{a,v}\,d\phi_{a,v}. \tag{13}$$

The fundamental differences between the boundary value problem in the foregoing formulation and that in Part I are (i) axial conduction is considered in the tissue region; (ii) the cross-sectional area of the tissue cylinder, the vessel radius, and the blood flow velocity can change in the axial direction; (iii) there is an axial temperature variation on the tissue cylinder surface; and (iv) the effect of blood bleedoff from the SAV vessels on the tissue temperature field is described by a Pennes-like source term developed in Part I. These will substantially change the boundary value problem in the axial direction without significantly changing the boundary value problem in the cross-sectional plane. The local tissue temperature on the outer boundary of the tissue cylinder $T^*_{t\text{local}}(z)$ is prescribed. This determines $F(z)$.

4 Solutions for the Countercurrent Flow

A theoretical solution to the complicated boundary value problem summarized in Section 3 can be obtained by modifying the solution procedure outlined in Wu et al. [23]. The simplifications introduced in the governing equations and the boundary conditions enable us to separate the variables and solve the boundary value problem in the cross-sectional plane independent of that in the axial direction. Using this approach, the axial interaction between vessels is reduced to a coupled system of two ordinary differential equations for the variation of the axial bulk temperatures in the SAV vessel pair.

The solutions for $T_{a,v}$ and T_t are decomposed into a particular solution and a homogeneous solution. These solutions which satisfy Eqs. (9)–(10) and matching conditions Eq. (11) are

$$\begin{bmatrix} T_a \\ T_v \\ T_t \end{bmatrix} = \begin{bmatrix} T_h \\ T_h \\ T_h \end{bmatrix} + [M]_{3\times 2}\begin{bmatrix} \dfrac{d(T_{ab}+F)}{dz} \\ \dfrac{d(T_{vb}+F)}{dz} \end{bmatrix} + \left\{\frac{1}{4}\left[-\frac{d^2F}{dz^2}-(T_{ab}-F)BP\right]\right\} \times \begin{bmatrix} 2a_a^2\ln\left(\dfrac{r_a}{a_a}\right)+a_a^2+s_a^2-2r_a s_a\cos\phi_a-R_t^2 \\ 2a_v^2\ln\left(\dfrac{r_v}{a_v}\right)+a_v^2+s_v^2-2r_v s_v\cos\phi_v-R_t^2 \\ R^2-R_t^2 \end{bmatrix}. \tag{14}$$

The third matrix on the right side of Eq. (14) arises from the axial conduction in the tissue region and the source term. The third group of terms in the expressions for T_a and T_v are harmonic and satisfy the matching conditions on the vessel surfaces, while the third group of terms in the expression for T_t satisfies the outside boundary condition at $R=R_t$. $[M]_{3\times 2}$ is a 3 by 2 matrix defined as

$$[M]_{3\times 2} = \begin{bmatrix} u_a\left(r_a^2-\dfrac{1}{4}\dfrac{r_a^4}{a_a^2}-\dfrac{3}{4}a_a^2\right) & -u_a a_v^2\ln\dfrac{r_v}{a_v} \\ u_v a_a^2\ln\dfrac{r_a}{a_a} & u_v\left(-r_v^2+\dfrac{1}{4}\dfrac{r_v^4}{a_v^2}+\dfrac{3}{4}a_v^2\right) \\ u_v a_a^2\ln\dfrac{r_a}{a_a} & -u_a a_v^2\ln\dfrac{r_v}{a_v} \end{bmatrix}\frac{\text{Pe}_0}{4} \tag{15}$$

and T_h is the homogeneous solution in the three regions. T_h is given by

$$T_h = u_v a_a^2\,\text{Pe}_0\left\{b_{a0}+\sum_{n=1}^{\infty} b_{an}R^n\cos[n(\phi-\pi)]\right\}\frac{d(T_{ab}+F)}{dz} + u_a a_v^2\,\text{Pe}_0\left\{-b_{v0}-\sum_{n=1}^{\infty} b_{vn}R^n\cos(n\phi)\right\}\frac{d(T_{vb}+F)}{dz}. \tag{16}$$

The solutions for the blood vessels and tissue satisfy the matching boundary conditions (Eq. (11)) on the vessel surfaces. Following a derivation similar to that presented in the Appendix of Wu et al. [23], one can solve for the coefficients b_{an} and b_{vn} by applying the boundary condition at $R=R_t$

$$b_{a0}=b_{v0}=b_0=-0.25\ln[R_t(z)/a(z)] \tag{17}$$

$$b_{an}=b_{vn}=b_n=0.25s^n(z)/[nR_t^{2n}(z)], \quad n=1,2,3,\ldots. \tag{18}$$

The temperature solutions in the artery and vein are used to determine the bulk temperatures (T_{ab} and T_{vb}). Substituting the vessel temperature expressions into Eq. (13) and evaluating the double integrals, one can relate the vessel bulk temperatures to their gradients:

$$T_{ab}=A_{11}\frac{d(T_{ab}+F)}{dz}+A_{12}\frac{d(T_{vb}+F)}{dz}+A_{13}\left[\frac{d^2F}{dz^2}+BP(T_{ab}-F)\right] \tag{19}$$

$$T_{vb}=A_{21}\frac{d(T_{ab}+F)}{dz}+A_{22}\frac{d(T_{vb}+F)}{dz}+A_{23}\left[\frac{d^2F}{dz^2}+BP(T_{ab}-F)\right] \tag{20}$$

where the coefficients A_{11-23} which depend on z and the local vascular geometry, are given by

$$\begin{aligned} A_{11}=-A_{22}&=\left[\sum_{n=0}^{\infty} b_n s^n-\frac{11}{96}\right]\text{Pe}_0\,ua^2 \\ &=-\text{Pe}_0\frac{ua^2}{4}\left\{\ln\left[\frac{R_t}{a}\left(1-\frac{s^2}{R_t^2}\right)\right]+\frac{11}{24}\right\} \\ A_{12}=-A_{21}&=\frac{1}{4}\text{Pe}_0\,ua^2\left[\sum_{n=0}^{\infty} b_n s^n\cos(n\pi)+\frac{\ln(l/a)}{4}\right] \\ &=\text{Pe}_0\frac{ua^2}{4}\left\{\ln\left[\frac{R_t/a}{l}\left(1+\frac{s^2}{R_t^2}\right)\right]\right\} \\ A_{13}&=A_{23}=0.25(R_t^2-s^2+0.5). \end{aligned} \tag{21}$$

It is relatively straightforward to apply the new model. The original boundary value problem has been reduced to two coupled first-order ordinary differential Eqs. (19) and (20) for the vessel bulk temperatures. The coefficients in (19) and (20) are given by

Table 1 Tissue temperature distribution

	Temperature Distribution	at $z^*=0$	at $z^*=L^*$
Arterial temperature $T^*_{ab}(z^*)$	model predicted	37(°C)	
Venous temperature $T^*_{vb}(z^*)$	model predicted		$T_{vb}(L)=0.3\,T_{ab}(0)$
Constant $T^*_{t\text{local}}(z^*)$	any value between 30–36(°C)	30–36(°C)	30–36(°C)
Linearly decreased $T^*_{t\text{local}}(z^*)$	$(30-36)z^*/L^*+36$ (°C)	36(°C)	30(°C)
Nonlinearly distributed $T^*_{t\text{local}}(z^*)$	$(30-36)z^{*2}/L^{*2}+36$ (°C)	36(°C)	30(°C)

the algebraic expressions in Eqs. (17), (18), and (21), which describe the thermal interaction in the cross-sectional plane. In principle, the axial dependence of the vessel bulk temperatures can be obtained once the appropriate boundary conditions in the axial direction as well as the function $F(z)$ are specified. One of the boundary conditions is the artery inlet temperature $T^*_{ab0}=37$ °C at $z=0$ and its dimensionless value can be determined according to the dimensionless temperature definition, while the other is the relationship between vessel bulk temperatures at $z=L$ which is determined in Part I [18]. The difference between $T^*_{ab}(L^*)$ and $T^*_{vb}(L^*)$ is equal to 0.6~0.8 times $T^*_{ab}(L^*)-T^*_{t\text{local}}(L^*)$. Converting this relationship into the definitions of the dimensionless variables, one obtains $T_{vb}(L)=0.2\sim0.4\,T_{ab}(L)$. In this paper an average value of 0.3 is used for $T_{vb}(L)$.

5 Results

5.1 Temperature Decay in SAV Vessels for Two Branching Patterns. We considered three special cases where constant, linearly decreasing or quadratically distributed local tissue temperature distributions are used as the input for $F(z)$ in the model. These three temperature variations are summarized in Table 1. The arterial temperature at the entrance, T^*_{ab0}, is equal to the body core temperature (37°C). Under hyperemic conditions, which may be induced by vasoactive drugs, it is reasonable to assume that only small temperature variations exist within the limb and thus, $T^*_{t\text{local}}(z^*)$ should be close to the body core temperature. However, large tissue temperature variations may occur under normal physiological conditions. The tissue temperature is assumed to decrease from 36°C to approximately 30°C as one proceeds from the center of the limb to the periphery.

All the other parameters and thermal properties are taken from the literature and are listed in Table 2. The blood velocity is proportional to the vessel radius as required by Murray's law. The radial size of the tissue cylinder R^*_{t0} was determined by requiring that the blood perfusion rate in the pure perfusion pattern for the normal conditions be equal to $\omega=3$ ml/100g/min, i.e., $\omega=\pi a^{*2}_0 u_0/\pi R^{*2}_{t0}L^*$. This blood perfusion value is equivalent to 0.0005 s^{-1} if the blood density is equal to 1000 kg/m^3. Previous experimental studies by Song et al. [15] suggested an eightfold increase in the blood flow rate when the vessel was manipulated from a constricted to a fully dilated condition using vasoactive drugs. Two physiological conditions were considered: (1) a normal condition: $\omega=3$ ml/100 g/min; and (2) a hyperemic condition: $\omega=24$ ml/100g/min corresponding to drug induced vasodilation. L^* is the distance over which the SAV vessel pair bifurcates from 1000 to 300 μm in diameter under normal conditions and was calculated from Eq. (6). We shall examine how blood temperature decays in the countercurrent vessel pair over a distance of $L^*=12$ cm for the two vessel branching patterns shown in Fig. 2.

For convenience the dimensionless temperatures in Figs. 4–9 are defined as

$$T_{ab,vb,t,t\text{local}}(z)=\frac{T^*_{ab,vb,t,t\text{local}}(z^*)-T^*_{t\text{local}}(L^*)}{T^*_{ab0}-T^*_{t\text{local}}(L^*)}. \qquad (22)$$

Accordingly, the dimensionless arterial temperature at $z=0$ is always equal to 1. A calculated dimensionless temperature equal to zero implies a temperature equal to the surface temperature of the tissue cylinder at $z^*=12$ cm.

Figure 4 shows the dimensionless temperature distributions in the SAV artery and vein for the pure branching pattern for both the normal and hyperemic conditions. Note that in this first calculation the tissue temperature at the cylinder surface $T^*_{t\text{local}}(z^*)$ is uniform in the axial direction. At the end of the cylinder ($z^*=12$ cm), the arterial blood nearly equilibrates with the local tissue temperature under normal conditions (thin solid line). However, for hyperemic conditions, the dimensionless arterial temperature decays only 10 percent at $z^*=12$ cm (heavy solid line). This is expected since for hyperemic conditions the blood flow rate is higher and results in less heat loss from the blood vessels. Notice also that the venous rewarming of the blood is smaller for the hyperemic conditions. From an energy balance point of view, heat lost from the SAV artery by conduction through the artery wall must enter either the tissue cylinder or its countercurrent vein. Therefore, the temperature increase in the SAV vein is always smaller than the temperature decrease in the SAV artery unless the tissue cylinder is infinitely large.

For the pure perfusion pattern shown in Fig. 5, the dimensionless arterial temperature defined in Eq. (22) decreases to 0.23 and 0.92 at $z^*=12$ cm for normal and hyperthermia conditions, respectively. Note that R^*_t is axially uniform in the pure perfusion

Table 2 Thermal properties and geometric parameters

	Pure Branching Pattern	Pure Perfusion Pattern
SAV vessel radius a^*_0	normal: $a^*(0)=500$ μm, $a^*(L^*)=150$ μm hyperemic: $a^*(0)=1000$ μm, $a^*(L^*)=300$ μm	
SAV vessel length L^*	12 cm	
Blood perfusion rate ω (for pure branching pattern)	normal: 3 ml/100 g/min or 0.0005 s^{-1}; hyperemic: 24 ml/100 g/min or 0.004 s^{-1};	
Vessel eccentricity s^*_0	normal: $s^*_0=625$ μm; hyperemic: $s^*_0=1250$ μm	
Blood flow velocity u^*_0	normal: $u^*_0=100$ mm/s; hyperemic: $u^*_0=200$ mm/s	
Tissue cylinder radius R^*_{t0}	$R^*_{t0}=20.14$ mm	
Constant C^* (Eq. (7))		$C^*=123.3$ mm
Density ρ_f	1000 kg/m^3	
Specific heat C_f	3600 J/kg K	
Thermal conductivity k_f	0.5 J/mK	

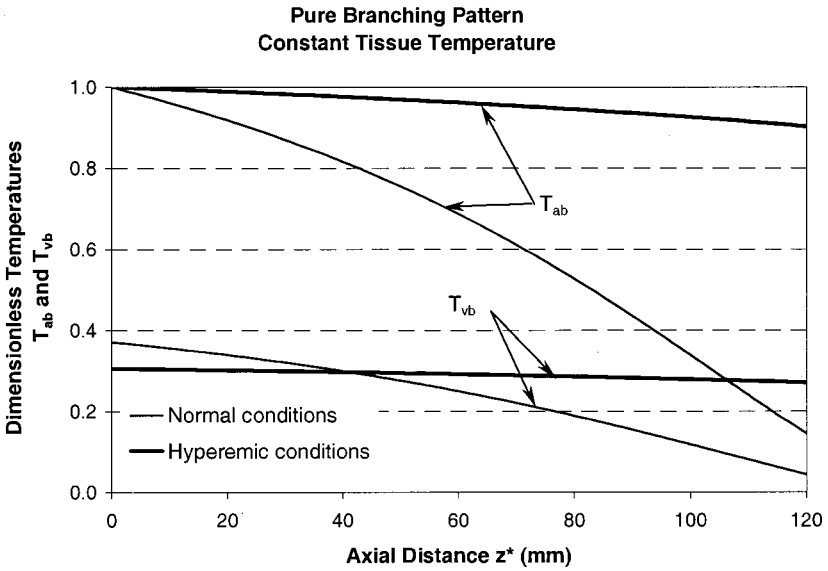

Fig. 4 Axial temperature distributions in the SAV artery and vein for the pure branching pattern under both normal and hyperemic conditions

pattern while it decays in the axial direction in the pure branching pattern. If one compares the results given in Figs. 4 and 5, it can be found that less heat is lost from the SAV artery in the pure perfusion pattern and, thus, a smaller temperature decay is observed than that in the pure branching pattern. Another interesting observation from Figs. 4 and 5 is that, unlike the pure branching pattern, the temperature increase in the vein in the pure perfusion pattern can be either larger or smaller than the temperature decrease in the artery depending on the blood perfusion rate. The fundamental difference between the two branching patterns is the bleedoff from the SAV vessels in the pure perfusion pattern. The total energy lost in the arterial side is not directly proportional to the temperature difference between two axial locations. Energy leaving the SAV artery consists of both the conduction loss from its surface and the advection due to the bleed off. Both conduction and advection contribute to the rewarming of the countercurrent SAV vein. The venous temperature increase can be larger than the artery temperature decay, if $T_{vb}(L)$ is smaller than T_{ab0}. This is more pronounced for the hyperemic condition since the bleedoff is significant.

The effect of the axial tissue temperature variation on the axial arterial temperature decay is shown in Figs. 6–9. Figure 6 is for the pure branching pattern under normal conditions. Here the curves represent three tissue temperature profiles. The heavy solid line is for a uniform $T_{t\text{local}}$, a linearly decreasing $T_{t\text{local}}$ is denoted by the thin solid line, while a nonlinearly distributed $T_{t\text{local}}$ is represented by the dashed line. For the normal condition, the axial tissue temperature variation has a modest effect on the arterial temperature profile; while its effect is smaller for the total heat loss from the artery for the pure branching pattern at $x=L$. In contrast, for hyperemic conditions shown in Fig. 7, the arterial temperature profiles vary little (<5 percent) with the tissue temperature variation. Similar conclusions can be drawn for the pure perfusion pattern (Figs. 8 and 9). Variations in the temperature at

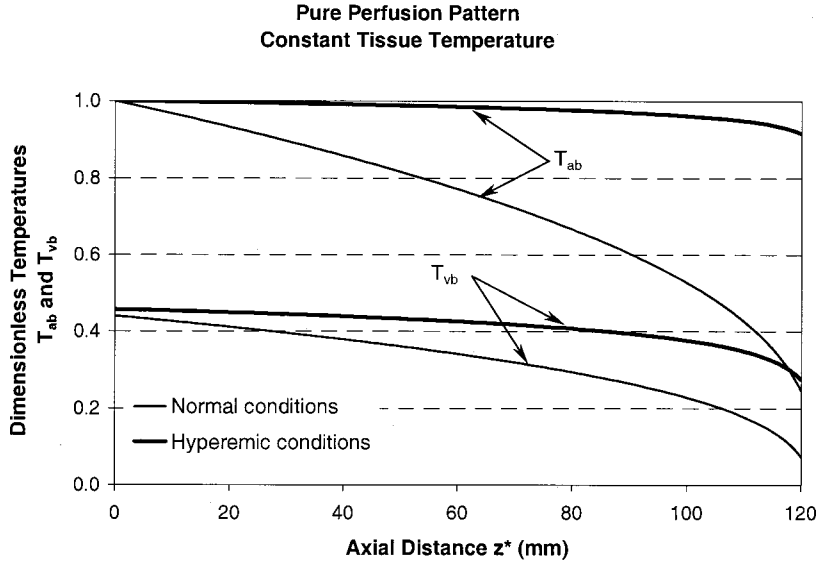

Fig. 5 Axial temperature distributions in the SAV artery and vein for the pure perfusion pattern under both normal and hyperemic conditions

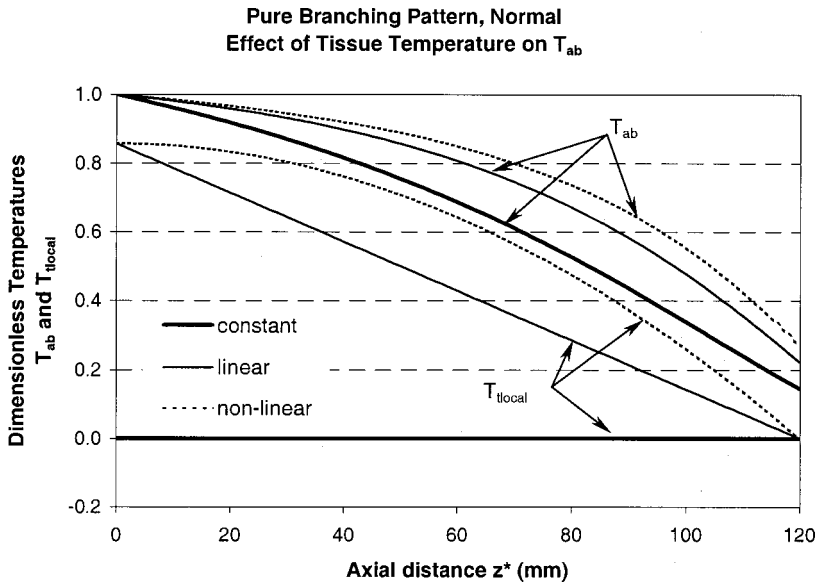

Fig. 6 Effect of the temperature variation at the tissue cylinder surface on the temperature decay in the SAV artery under normal conditions for the pure branching pattern

the tissue cylinder surface result in less than 10 percent and 2 percent changes in the arterial temperature at $z^*=12$ cm for this pattern under normal and hyperemic conditions, respectively.

The present model for the SAV vessels makes it possible to evaluate the contribution of various size vessels to the total blood-tissue heat exchange under different physiological conditions. For the pure branching pattern, the total heat released from the blood vessels to the tissue is proportional to the temperature difference between T_{ab} and T_{vb} at the SAV vessel entrance. Similarly, the heat released from the *s* vessels to the tissue is proportional to $T_{ab}-T_{vb}$ at the SAV vessel exit. The percentage of heat released from the blood vessels prior to the *s* vessels is represented by $1-[T^*_{ab}(L^*)-T^*_{vb}(L^*)]/[T^*_{ab}(0)-T^*_{vb}(0)]$. The larger this value, the greater the fractional heat release by the SAV vessels compared to the smaller downstream *s* vessels. Table 3 summarizes the percentage of heat released in the SAV vessels to the total vessel-tissue heat exchange. One observes that for hyperemic conditions, far less heat is released in the SAV vessels than in the smaller downstream *s* vessels and their subsequent branches. Under normal conditions, more than 48 percent of the total heat exchange occurs in the region containing large SAV vessels for the pure branching pattern. However, less than 10 percent is released in the SAV vessels for the assumed hyperemic conditions. The local tissue temperature variation does affect the contribution of different sized vessels to the total blood-tissue heat exchange. Its effect is more pronounced for the normal condition than for the hyperemic condition.

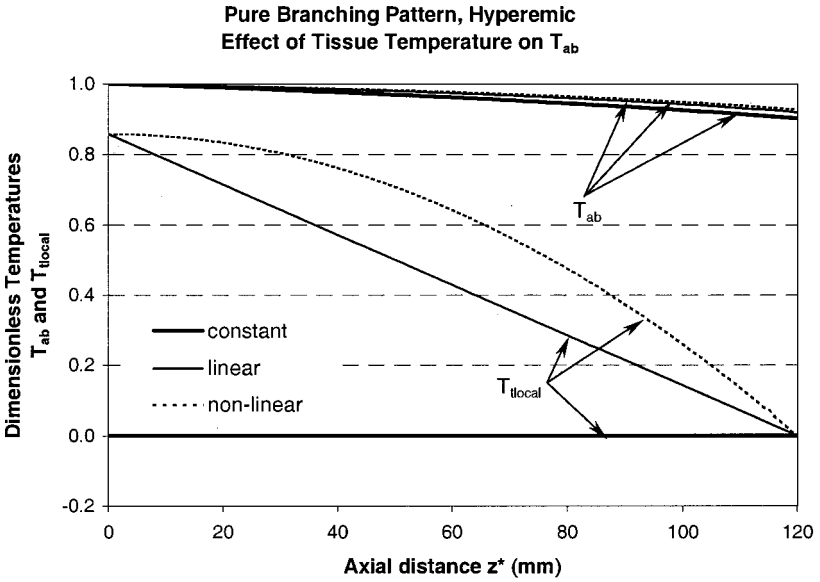

Fig. 7 Effect of the temperature variation at the tissue cylinder surface on the temperature decay in the SAV artery under hyperemic conditions for the pure branching pattern

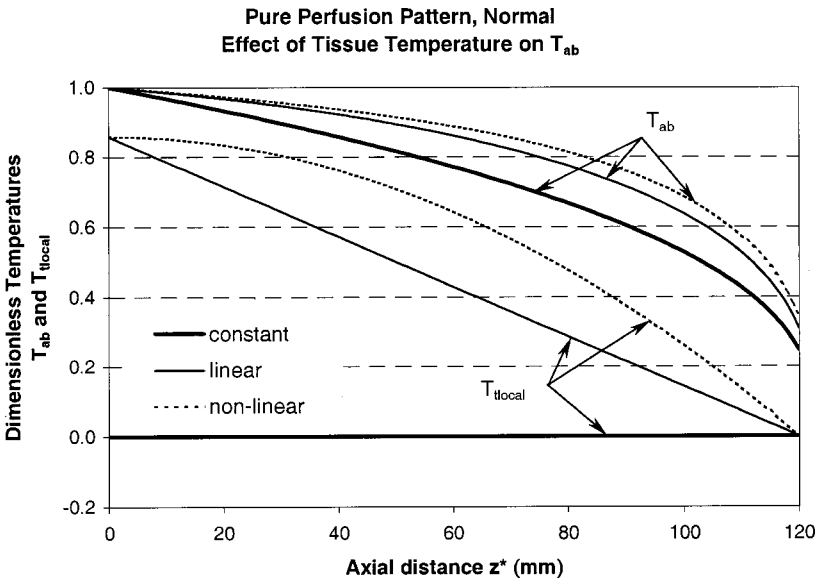

Fig. 8 Effect of the temperature variation at the tissue cylinder surface on the temperature decay in the SAV artery under normal conditions for the pure perfusion pattern

5.2 Temperature Decay in the SAV Vessels in Human Limb. Based on results obtained in Section 5.1 for the two limiting vessel branching patterns, we shall now consider the temperature decay in the SAV vessels of a human limb. Unfortunately, no detailed anatomic data are available for blood vessels larger than 300 μm diameter in the human limb, equivalent to the Myrahage and Eriksson data for the *s* vessel tissue cylinder in Part I [18]. We assume that for the blood vessels to be space filling, the vascular structure reproduces itself on a larger scale. As sketched in Fig. 1, the SAV vessels bifurcate from the large muscular branches and then run roughly parallel to the skin surface. Each SAV vessel pair supplies a large tissue cylinder of uniform radius, via several *P* vessels and their subsequent *s* vessels and *t* vessels. The temperature variation in the muscular branches from the major supply artery and vein for the limb is assumed to be small compared to that in the SAV vessels. This assumption is due to the large size of the muscular branches and is based on our calculation in Section 5.1 where less than 10 percent of the temperature decay occurs in vessels between 1000 and 800 μm in diameter. The temperature at the SAV tissue cylinder surface is assumed to be uniform since it is parallel to the skin surface. Thus, in this section, the temperature decay in the SAV vessels is determined from the thermal interaction between a tapered vessel pair with uniform bleed off, and a uniform radius tissue cylinder with constant surface temperature.

Several parameters such as the tissue cylinder radius, SAV ves-

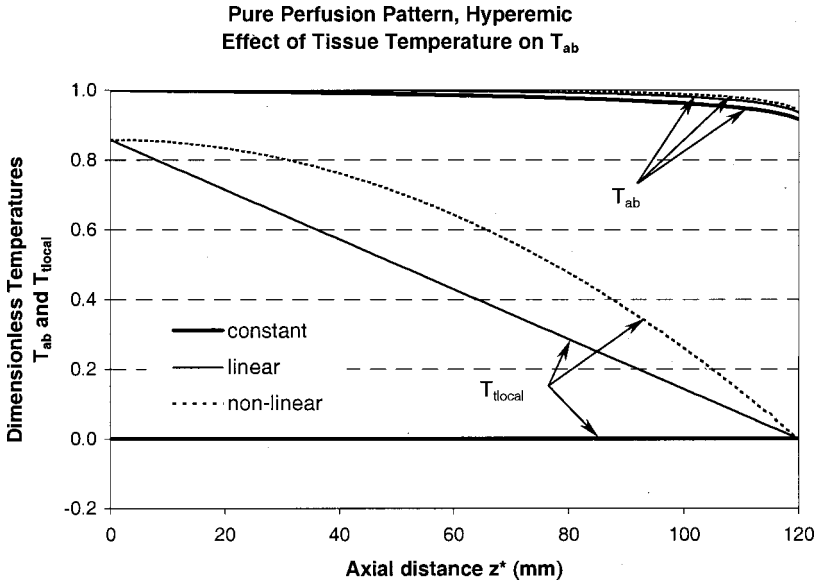

Fig. 9 Effect of the temperature variation at the tissue cylinder surface on the temperature decay in the SAV artery under hyperemic conditions for the pure perfusion pattern

Table 3 Percentage of total heat loss prior to the *s* vessels

Conditions	Pattern	Uniform T_{tlocal} (percent)	Linearly Decreased T_{tlocal} (precent)	Nonlinear T_{tlocal} (precent)
Normal	pure branching	83.8	64.8	48.5
Hyperemic	pure branching	9.0	4.1	2.2

sel size at the entrance and exit, and the tissue cylinder length, are needed to simulate the temperature field. In Myrahage and Eriksson's [19] description of the *s* vessel tissue cylinder, many muscle fibers (100 or more) supplied by the *t* vessels combine to create one *s* vessel tissue cylinder. In the same manner, we propose that many *s* vessel tissue cylinders combine to provide a larger tissue cylinder supplied by the SAV vessel pair. The SAV vessels play the same role as the *s* vessels in our smaller *s* vessel tissue cylinder except that they are one order of magnitude larger. Similarly, the *P* vessels are equivalent to the *t* vessels except that the *P* vessels are one order of magnitude larger. The average radii of the *P* and *t* vessels in the different muscle tissues listed in Table 1 in Part I [18] are 110 μm and 12 μm, respectively. Applying a similar scaling law, one finds that the SAV vessel at its entrance is approximately 350 μm in radius if the *s* vessel radius has an average value of 38 μm. The SAV tissue cylinder length is half the distance between any two adjacent large muscular branches. Gray's anatomy text indicates that there are typically three or four large muscular branches in the human upper limb [24]. The distance between any two adjacent muscular branches will be approximately 16 cm if the length of the upper limb is 48 cm. The blood flow in the SAV artery supplies a tissue cylinder 8 cm in length. The total blood flow rate Q in the SAV artery is then calculated as 1.61 ml/min. Thus, the tissue cylinder radius can be determined by requiring the average blood perfusion rate be equal to 3 ml/100g/min under normal conditions. This will lead to $R_{t0} = 14.6$ mm.

Table 4 Vascular parameters and blood flow in human limb

	a_0^* (μm)	a_e^* (μm)	R_t^* (mm)	C^* (mm)	L^* (mm)	Q_0 (ml/min)	ω (ml/100g/min)
Normal	350	150	14.6	86.8	80	1.61	3
Hyperemic	700	300	14.6	86.8	80	12.9	24

Another parameter that needs to be determined is the SAV vessel size at the midpoint of the tissue cylinder where two SAV vessel pairs running in opposite directions meet. Myrahage and Eriksson [19] observed that the average distance between any two adjacent *P* vessels is about 12 mm; thus, there are an average of 13 (16 cm/12 mm) *P* vessels between major muscular branches. The blood flow rate in the central *P* vessel at the midpoint of the SAV tissue cylinder should be equal to Q_e, the blood flow rate in the SAV at the juncture of the two SAV vessel pairs. If one assumes that all the *P* vessels have the same blood supply, the blood supply in each *P* vessel will be 1/13 of the blood supply to the SAV artery at its entrance. Using Murray's law, one finds that the blood velocity u is proportional to the vessel radius. This requires that the SAV vessels be approximately 300 μm in diameter at the end of the large tissue cylinder. Under hyperemic conditions the SAV vessels will dilate 100 percent to achieve a local blood perfusion rate of 24 ml/100g/min. Table 4 lists all the estimated parameters.

Figures 10 and 11 show model predictions for the temperature decay along the SAV artery and vein, respectively, in a human limb for different blood perfusion rates ranging from normal conditions of 3 ml/100g/min to hyperemic conditions of 24 ml/100g/min. It is shown that up to 90 percent thermal equilibration can be achieved in SAV arterial blood depending on the blood perfusion rate. The SAV artery has a longer thermal equilibration length when the blood flow is higher and only 20 percent thermal equilibration is reached under hyperemic conditions of 24 ml/100g/min. In contrast to the arterial temperature decay, the local blood perfusion rate seems to play a minor role in the venous return temperature since the dimensionless venous return temperature in the SAV vein is ~0.4 independent of ω, as shown in Fig. 11. The model predicts that in the human limb, 40 percent of the heat released from the artery is recaptured by its countercurrent SAV vein. The independence of the venous return on the blood perfusion rate is similar to that found for the *s* vessel tissue cylinder in part I [18], and will be discussed more fully in the next section.

6 Discussion

In this study a vascular model is developed to simulate the thermal equilibration in the SAV artery and vein. It is shown that

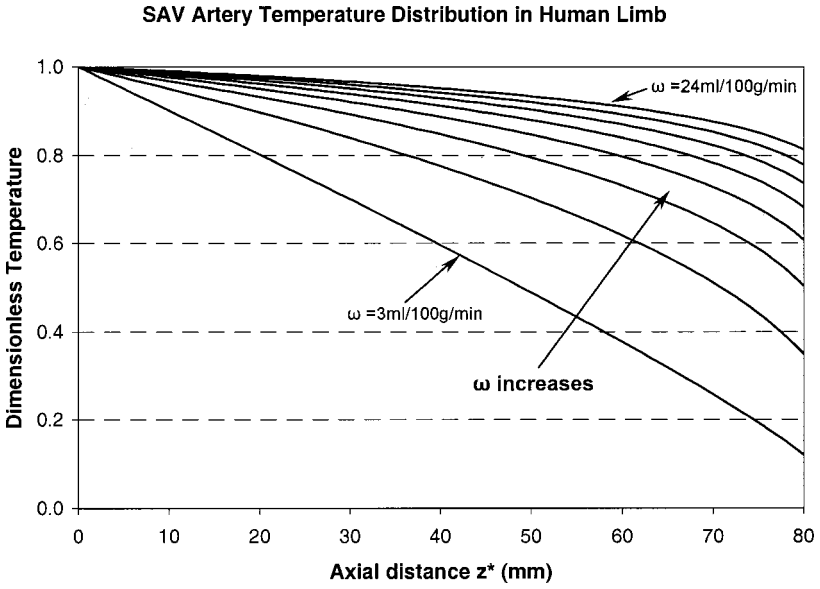

Fig. 10 Temperature decay in the SAV artery in a human limb

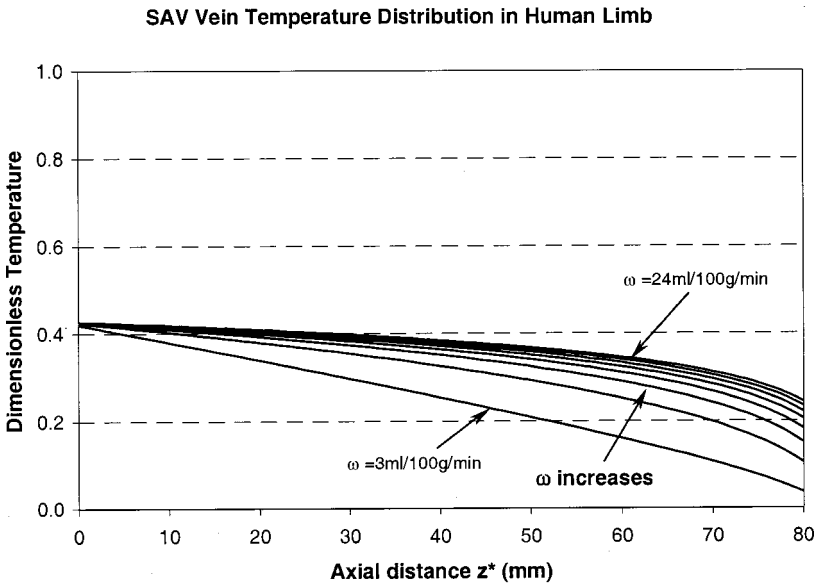

Fig. 11 Temperature decay in the SAV vein in a human limb

both the vessel branching pattern and the physiological conditions are the main factors affecting the temperature decay in the SAV vessels. Under normal or hyperemic conditions without external heating, the local tissue temperature variation seems to play a minor role in determining the temperature decay in the SAV artery. The current results provide two limits for the possible temperature variation in the SAV artery. This SAV arterial temperature decay, as well as the correction coefficient defined in Part I of this study, can be used in the modified perfusion source term to more accurately estimate the net heat release from the countercurrent *s* vessel pair in the *s* tissue cylinder. One of the shortcomings of all the continuum models is that they are incapable of accurately predicting point-to-point temperature variation in the vicinity of large blood vessels. This study shows that for hyperemic conditions encountered in hyperthermia it is a reasonable assumption to use the body core temperature as the arterial inlet temperature in the modified perfusion source term for the *s* vessel tissue cylinder. The lack of thermal equilibration will create large tissue temperature gradients in the vicinity of 300~1000 μm diameter vessels.

The search for a suitable energy equation that accurately reflects the heat released or removed by the blood has been a central theme in bioheat transfer research for nearly half a century. The individual *s* vessel muscle tissue cylinder defined in the anatomical studies of Myrhage and Eriksson [19] is the largest repetitive unit that is common to nearly all muscle tissue whether the tissue is deep or peripheral. This suggested that a single bioheat transfer equation could be derived and applied to all muscle tissue which was based on this anatomical unit. In Part I of this study, a modified Pennes source term was derived in which a correction coefficient was defined to account for the heat loss recaptured by the countercurrent *s* vein. Roemer and Dutton [25] have also proposed a modified Pennes-like perfusion term based on a generic tissue model for convective energy exchange. Although it is nontissue specific, the correction coefficient is rather complicated and hard to evaluate. This coefficient depends on the total heat transfer coefficients between tissue and blood in artery and vein, respectively, which vary from generation to generation with the flow. The correction coefficient also depends on the local venous return, and the thermally significant arteries and veins. In comparison, the model developed in this study gives a simple correction coefficient for the Pennes source term, which ranges from 0.6 to 0.8 for muscle tissues. This correction is much easier to apply in practice. In the present paper the temperature distribution in the SAV artery, or the entrance temperature for the *s* vessel tissue cylinder that appears in the new modified source term in Part I of this study, was calculated for two vascular branching patterns. These patterns represent two limits of possible thermal interaction between SAV blood vessels and tissue. Thus, these two cases provide the reasonable range of temperature variation along the SAV artery that one would anticipate for different physiological conditions. It is found that for both vessel branching patterns, at least 77 percent of the thermal equilibration is achieved in the SAV artery before it enters the *s* vessel tissue cylinder for normal physiological conditions. However, for hyperemic conditions most of the heat transfer from the countercurrent blood vessels to the local tissue occurs in the tissue region containing smaller blood vessels. There is a smaller temperature variation in the SAV arterial blood compared to that under normal conditions. The dimensionless arterial temperature in the SAV vessels is almost a constant for both branching patterns during hyperemia. Thus, for this case the arterial temperature appearing in the modified source term can be treated as a constant whose value is close to the body core temperature as noted earlier.

The heat exchange between countercurrent microvascular artery-vein pairs has attracted widespread attention since the combined theoretical and experimental studies by the authors [3] first suggested that this might be the dominant heat transfer mechanism in local microvascular blood-tissue heat transfer. The Weinbaum-Jiji bioheat transfer equation [26] was developed based on the incomplete countercurrent exchange that took place between the paired vessels. However, subsequent studies [14,15,27] showed that the limit for the validity of the expression for the effective conductivity describing these vessels was limited to vessel pairs of <200 μm diameter. The current study can predict axial temperature distributions in countercurrent vessel pairs ranging from 300 to 1000 μm in diameter and is also able to evaluate the deviation of the thermal interaction from perfect countercurrent heat exchange. The model predicts that for a human limb 40 percent of the heat lost from the SAV arteries and their branches is recaptured by their countercurrent vein. The thermal interaction between the SAV vessels is thus, far from being perfect countercurrent heat exchange. We also observe that for these larger thermally significant vessels the gradient of the mean tissue temperature does not follow the gradient of the mean blood temperature. This simulation confirms the conclusion of our experimental studies [15,27] that the Weinbaum-Jiji equation breaks down in tissue regions with blood vessels >200 μm diameter.

The 40 percent venous rewarming in a human limb is a com-

bined venous rewarming that includes both the SAV and *s* vessel tissue cylinders, since the thermal interaction in the *s* vessel tissue cylinder was included in the boundary condition applied at $x=L$, the end of the SAV vessel tissue cylinder. The fact that the venous return temperature does not depend on ω is not a surprising result. This was previously observed for the *s* vessel tissue cylinders in Weinbaum et al. [18]. This behavior is the consequence of several assumptions used in the model. First, there is no axial temperature gradient in the SAV tissue cylinder. Thus, the countercurrent heat exchange is the only thermal driving force for the blood-tissue heat transfer. Second, the same mass flow is assumed in each vessel of the SAV vessel pair. Finally, if one combines the boundary value problems for both the SAV and *s* vessel tissue cylinders, the flow must vanish at the end of the combined tissue cylinder where both the artery and vein temperatures are equal to the local tissue temperature. In contrast, if there is an axial thermal gradient in the tissue cylinder, the blood flow rate can play a significant role in the venous rewarming. As shown in Table 3, the local tissue temperature profile has a significant effect on the redistribution of the thermal interaction in different tissue regions. The percentage of the total heat loss prior to the *s* vessels is decreased by 35 percent when the uniform tissue temperature distribution is replaced by a quadratically distributed local tissue temperature for the normal perfusion rate.

In summary, this study presents a new theoretical framework to investigate axial temperature variations along countercurrent blood vessels from 300 to 1000 μm diameter in skeletal muscle. The thermal interaction between the blood vessel pair and the surrounding tissue was investigated for two vascular branching patterns. It was shown that temperature variations along these larger thermally significant vessels depend strongly on the vascular geometry and local blood perfusion rate. The arterial supply temperature to the *s* vessel tissue cylinders was evaluated and used in the modified perfusion source term in Part I of this study, to evaluate the relative contribution of the SAV vessels and the *s* vessels to the overall blood-tissue heat exchange.

Acknowledgment

This research was supported by a Whitaker Biomedical Research Grant to Liang Zhu.

Nomenclature

a = vessel radius
C = constant in Eq. (4)
C_f = specific heat of blood
k = thermal conductivity
l = vessel center to center spacing
L_i = vessel length in vessel generation i
L = total length of SAV vessels
Pe = blood flow Peclet number
r = radial coordinate
R = radial coordinate
R_t = radius of the tissue cylinder
s = vessel eccentricity
T_{ab0} = arterial blood temperature at its entrance
$T_{t\text{local}}$ = temperature at the tissue cylinder surface
u = flow velocity component in the axial direction in the blood vessels
x,y = Cartesian coordinates
ρ = density
ϕ = polar angle in cylindrical coordinate

Subscripts

a = artery
b = bulk
f = fluid in vessels
h = homogeneous solution
t = tissue
v = vein
0 = $z=0$

Superscripts

• = dimensional parameters and variables

References

[1] Chen, M. M., and Holmes, K. K., 1980, "Microvascular Contributions to Tissue Heat Transfer," Ann. N.Y. Acad. Sci., **335**, pp. 137–150.
[2] Pennes, H. H., 1948, "Analysis of Tissue and Arterial Blood Temperatures in the Resting Human Forearm," J. Appl. Physiol., **1**, pp. 93–122.
[3] Weinbaum, S., Jiji, L. M., and Lemons, D. E., 1984, "Theory and Experiments for the Effects of Vascular Microstructure on Surface Tissue Heat Transfer-Part I: Anatomical Foundation and Model Conceptualization," ASME J. Biomech. Eng., **106**, pp. 321–330.
[4] Baish, J. W., Ayyaswamy, P. S., and Foster, K. R., 1986, "Heat Transport Mechanism in Vascular Tissues: a Model Comparison," ASME J. Biomech. Eng., **108**, pp. 324–331.
[5] Baish, J. W., Ayyaswamy, P. S., and Foster, K. R., 1986, "Small-Scale Temperature Fluctuations in Perfused Tissue During Local Hyperthermia," ASME J. Biomech. Eng., **108**, pp. 246–250.
[6] Brinck, H., and Werner, J., 1994, "Estimation of the Thermal Effect of Blood Flow in a Branching Countercurrent Network Using a Three-Dimensional Vascular Model," ASME J. Biomech. Eng., **116**, pp. 324–330.
[7] Charny, C. K., Weinbaum, S., and Levin, R. L., 1990, "An Evaluation of the Weinbaum-Jiji Bioheat Equation for Normal and Hyperthermic Conditions," ASME J. Biomech. Eng., **112**, pp. 80–87.
[8] Crezee, J., Mooibroek, J., Lagendijk, J. J. W., and Van Leneuwen, G. M. J., 1994, "The Theoretical and Experimental Evaluation of the Heat Balance in Perfused Tissue," Phys. Med. Biol., **39**, pp. 813–832.
[9] Lemons, D. E., Chien, S., Crawshaw, L. I., Weinbaum, S., and Jiji, L. M., 1987, "The Significance of Vessel Size and Type in Vascular Heat Transfer," Am. J. Physiol., **253**, pp. R128–R135.
[10] Roemer, R. B., Moros, E. G., and Hynynen, K., 1989, "A Comparison of Bioheat Transfer and Effective Conductivity Equation Predictions to Experimental Hyperthermia Data," *Proceedings of ASME Winter Annual Meeting*, pp. 11–15.
[11] Valvano, J. W., Nho, S., and Anderson, G. T., 1994, "Analysis of the Weinbaum-Jiji Model of Blood Flow in the Canine Kidney Cortex for Self-Heated Thermistors," ASME J. Biomech. Eng., **116**, pp. 201–207.
[12] Xu, L. X., Chen, M. M., Holmes, K. R., and Arkin, H., 1991, "The Theoretical Evaluation of the Pennes, the Chen-Holmes and the Weinbaum-Jiji Bioheat Transfer Models in the Pig Renal Cortex," *Proceeding of ASME Winter Annual Meeting*, Atlanta, **189**, pp. 15–22.
[13] Crezee, J., and Lagendijk, J. J. W., 1990, "Experimental Verification of Bioheat Transfer Theories: Measurement of Temperature Profiles Around Large Artificial Vessels in Perfused Tissue," Phys. Med. Biol., **35**, No. 7, pp. 905–923.
[14] Song, J., Xu, L. X., Weinbaum, S., and Lemons, D. E., 1997, "Enhancement in the Effective Thermal Conductivity in Rat Spinotrapezius due to Vasoregulation," ASME J. Biomech. Eng., **119**, pp. 461–468.
[15] Song, J., Xu, L. X., Weinbaum, S., and Lemons, D. E., 1999, "Microvascular Thermal Equilibration in Rat Spinotrapezius Muscle," Ann. Biomed. Eng., **27**, pp. 56–66.
[16] Brinck, H., and Werner, J., 1994, "Efficiency Function: Improvement of Classical Bioheat Approach," J. Appl. Physiol., **77**, No. 4, pp. 1617–1622.
[17] Wissler, E. H., 1988, "Comments on Weinbaum-Jiji's Discussion of Their Proposed Bioheat Equation," ASME J. Biomech. Eng., **108**, pp. 355–356.
[18] Weinbaum, S., Xu, L. X., Zhu, L., and Ekpene, A., 1997, "A New Fundamental Bioheat Equation for Muscle Tissue: Part I—Blood Perfusion Term," ASME J. Biomech. Eng., **119**, pp. 278–288.
[19] Myrhage, R., and Eriksson, E., 1984, "Arrangement of the Vascular Bed in Different Types of Skeletal Muscles," Progress in Applied Microcirculation, **5**, pp. 1–14.
[20] He, Q., Zhu, L., Weinbaum, S., and Lemons, D. E., 2001, "Experimental Measurements of Temperature Variations Along Paired Vessels from 200 to 1000 μm in Diameter in Rat Hind Leg," ASME J. Biomech. Eng., in review.
[21] Whitmore, R. L., 1968, *Rheology of Circulation*, Pergamon Press, London.
[22] Zhu, L., and Weinbaum, S., 1995, "A Model for Heat Transfer from Embedded Blood Vessels in Two-Dimensional Tissue Preparations," ASME J. Biomech. Eng., **117**, pp. 64–73.
[23] Wu, Y. L., Weinbaum, S., Jiji, L. M., and Lemons, D. E., 1993, "A New Analytic Technique for 3-d Heat Transfer from a Cylinder With Two or More Axially Interacting Eccentrically Embedded Vessels With Application to Countercurrent Blood Flow," Int. J. Heat Mass Transf., **36**, pp. 1073–1083.
[24] Gray, H., 1974, "Anatomy, Descriptive and Surgical," 1901 Ed., Running Press, Philadelphia.
[25] Roemer, R. B., and Dutton, A. W., 1998, "A Generic Tissue Convective Energy Balance Equation: Part I—Theory and Derivation," ASME J. Biomech. Eng., **120**, pp. 395–404.
[26] Weinbaum, S., and Jiji, L. M., 1985, "A New Simplified Bioheat Equation for the Effect of Blood Flow on Local Average Tissue Temperature," ASME J. Biomech. Eng., **107**, pp. 131–139.
[27] Zhu, L., Weinbaum, S., and Lemons, D. E., 1996, "Microvascular Thermal Equilibration in Rat Cremaster Muscle," Ann. Biomed. Eng., **24**, pp. 109–123.